Optical addressing at the subwavelength scale

J. C. Weeber and A. Dereux
Laboratoire de Physique de l'Université de Bourgogne, Optique Submicronique, Boîte Postale 47870, F-21078 Dijon, France

Ch. Girard and G. Colas des Francs
Centre d'Elaboration des Matériaux et d'Etudes Structurales, 29 Rue Jeanne Marvig, Boîte Postale 4347, F-31055 Toulouse, France

J. R. Krenn
Institut für Experimentalphysik, Universität Graz, Universitätsplatz 5, A-8010 Graz, Austria

J. P. Goudonnet
Laboratoire de Physique de l'Université de Bourgogne, Optique Submicronique, Boîte Postale 47870, F-21078 Dijon, France
(Received 24 May 2000)

The Green dyadic formalism is applied to the study of the optical properties of dielectric subwavelength structures integrated in coplanar geometry. We first consider homogeneous wires with high refractive index featuring subwavelength cross sections. We show that such wires may have guiding properties and that they may be coupled with a local illumination produced by a focused Gaussian beam totally reflected at the substrate interface. When excited by the focused beam, these subwavelength optical waveguides (SOW's) provide a confined source of light that could be used to excite a single nanoscopic object. Well designed heteregeneous wires resulting from the alignment of dielectric particles separated from each other by a subwavelength distance are also found to propagate a Gaussian beam excitation over several micrometers. This propagation occurs with reasonable damping for incident beams in the visible frequency range. The computed transmission spectra of these heterowires may exhibit narrow gaps. Finally, we discuss the relation between the optical properties of the SOW and the calculated electromagnetic local density of states.

PACS number(s): 78.66.−w, 71.36.+c, 07.79.Fc

I. INTRODUCTION

The development of near-field optical microscopy techniques now allows mapping of the spatial distribution of the electromagnetic field intensity at the subwavelength scale [1]. In this context, these techniques may be used to check the operation of devices integrated in coplanar geometry and aimed at controlling the propagation of light at the submicrometer scale. Such devices might be of experimental interest for addressing optically single nanoscopic objects deposited on a substrate. Recently, several studies dealing with electromagnetic energy transfer assisted by subwavelength-sized structures were reported. Takahara *et al.* [2] investigated theoretically the propagation of a model optical beam with a subwavelength diameter using a metallic core cylindrical waveguide. Quinten *et al.* [3] have suggested theoretically that the *dipole-dipole* coupling between metallic clusters could sustain efficient transfer of electromagnetic energy along a linear chain of silver nanoparticles. Numerical work has demonstrated the propagation of local illumination by exploiting the plasmon polaritons sustained by metallic nanowires [4].

Concerning nonmetallic structures, it has been suggested that illuminating under total internal reflection a low-index medium inserted between two semi-infinite higher-index transparent media provides an operational, albeit incomplete, photonic band gap [5]. One can then think of introducing subwavelength structures for transferring light through this kind of operational gap. Recently, numerical simulations have strengthened this appealing idea by introducing dielectric particles aligned to build heterowires in the low-index gap so as to link optically both higher-index media by exploiting an optical resonant tunneling effect. Such structures were predicted to be efficient for transferring light through the operational gap by exploiting the resonant tunneling effect [6,7]. Inspired by these works, the optical coupling between two channel waveguides using an array of periodic mesoscopic pillars was observed very recently [8].

In this paper, we demonstate theoretically how finite-length subwavelength optical waveguides (SOW's) integrated in coplanar geometry can guide the incident light of *a focused beam*. Such devices of subwavelength cross section are deposited on a flat transparent substrate. They are made of materials having high refractive indices. The SOW's are excited by a three-dimensional (3D) Gaussian beam which is incident on the transparent substrate in such a way that it is totally reflected when there is no structure deposited on the surface of the said substrate. The optical properties of the SOW are analyzed on the basis of near-field optical intensity maps computed with the Green dyadic technique (GDT). This intensity is proportionnal to the signal that can be detected by a photon scanning tunneling microscope operating in constant height mode and equiped with a dielectric tip [1]. Together with a brief summary of the GDT, the modeling of the 3D Gaussian beam is described in Sec. II. The numerical results obtained for SOW's with homogeneous or periodically modulated dielectric functions are discussed, respectively, in Secs. III and IV. Specifically, Sec. IV details the near-field transmission spectrum of a finite-length linear chain of dielectric particles. Finally, Sec. V discusses the

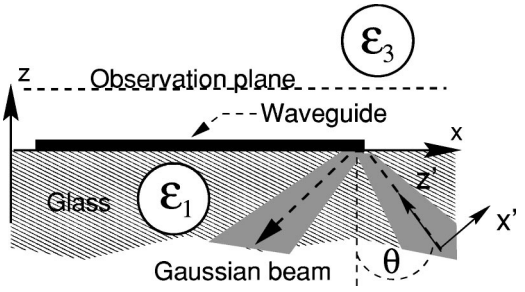

FIG. 1. Definition of the parameters of the computation. A SOW (dielectric function ε_2) lying on the surface of a substrate (dielectric function ε_1) is illuminated by a Gaussian beam reflected at the interface between the substrate and the outside medium (dielectric function ε_3).

relationship between the optical properties of the SOW and the electromagnetic local density of states (LDOS).

II. THEORETICAL BACKGROUND

We use Green's dyadic technique which has proved to be reliable in investigating the optical properties of low-symmetry systems near surfaces [9,10]. In this section, we summarize the principle of the method before describing the model of the field associated with the incident 3D Gaussian beam used to excite a SOW.

A. Lippmann-Schwinger equation

Figure 1 depicts a schematic view of the reference geometry. A SOW, with a volume Ω, is fabricated on a transparent substrate. A monochromatic 3D Gaussian beam with an angular frequency ω in vacuum propagating along the z' axis locally excites one end of the SOW. To study the guiding properties of the SOW, we compute the spatial distribution of the electric field intensity $|\vec{E}(\vec{r},\omega)|^2$ in an observation plane parallel to the surface. A general solution for the field $\vec{E}(\vec{r},\omega)$ is given by the implicit Lippmann-Schwinger equation:

$$\vec{E}(\vec{r},\omega)=\vec{E}_0(\vec{r},\omega)+\int_\Omega d\vec{r}'\,\overleftrightarrow{G}_{\mathrm{ref}}(\vec{r},\vec{r}',\omega)V\vec{E}(\vec{r}',\omega), \quad (1)$$

where $V=(\varepsilon_3-\varepsilon_2)\omega^2/c^2$. ε_3 and ε_2 denote, respectively, the dielectric function of the upper half space and the dielectric function of the SOW while, as usual, ω is the angular frequency and c is the speed of light in vacuum. The Green dyadic $\overleftrightarrow{G}_{\mathrm{ref}}(\vec{r},\vec{r}',\omega)$ describes the field observed at $\vec{r}$ if a fluctuating point source, located at $\vec{r}'$, interacts with the reference system, which is defined here to be the bare interface of the substrate (i.e., not including the SOW). The formula of $\overleftrightarrow{G}_{\mathrm{ref}}(\vec{r},\vec{r}',\omega)$ may be found in several references [11,12] and care must be used in handling the so called ''self-terms'' arising when $\vec{r}=\vec{r}'$ [13]. In our case, $\vec{E}_0(\vec{r},\omega)$ is the electric field of the incident Gaussian beam decaying in medium ε_3.

Applying the GDT to compute the total field $\vec{E}(\vec{r},\omega)$ requires discretization of the direct space. The SOW is thus modeled by a finite number of small polarizable pieces of matter (cells). If the dimensions of the cells are small compared to the effective wavelength of the medium, the electromagnetic field is supposed to be constant over the volume of each cell. The discretized form of Eq. (1),

$$\vec{E}(\vec{r},\omega)=\vec{E}_0(\vec{r},\omega)+Vv\sum_{\vec{r_k}\in\Omega}\overleftrightarrow{G}_{\mathrm{ref}}(\vec{r},\vec{r_k},\omega)\vec{E}(\vec{r_k},\omega), \quad (2)$$

where v denotes the volume of one cell and $\vec{r_k}$ the center position of the kth cell, may then be cast as a system of linear equations in which the unknowns are the values of the electric field $\vec{E}(\vec{r_k},\omega)$ inside each cell. This system is solved by standard algorithms.

B. Modeling a totally reflected 3D Gaussian beam

In order to solve Eq. (2), we have to provide an expression of the zeroth order solution $\vec{E}_0(\vec{r},\omega)$. This field corresponds to that of a three-dimensional Gaussian beam that is incident on the flat interface, i.e., in the absence of any structure deposited on the substrate. For the aim of this paper, we need to compute $\vec{E}_0(\vec{r},\omega)$ only for $\vec{r}$ coordinates located above the substrate. The electric field associated with this beam is expanded as a two-dimensional spectrum of plane waves so that, for an incident beam propagating in the (xOz) plane toward negative values of x (see Fig. 1), it reads

$$\vec{E}'_{\mathrm{inc}}(x',y,z')=\int_{-\infty}^{+\infty}d\alpha\int_{-\infty}^{+\infty}d\beta\,\vec{\xi}'_{\mathrm{inc}}(\alpha,\beta)\times\exp[i\alpha x'+i\beta y+i\gamma_{(\alpha,\beta)}(z'-z'_0)]. \quad (3)$$

In this last formula, we used a rotation around the y axis which defines Cartesian coordinates (x',y,z') such that the z' direction is parallel to the direction of propagation of the incident beam. In this system of coordinates, $(0,0,z'_0)$ locates the focal point of the Gaussian beam and the z' component of the wave vector $\gamma_{(\alpha,\beta)}$ of the incident beam is simply given by

$$\gamma_{(\alpha,\beta)}=\left(\varepsilon_1\frac{\omega^2}{c^2}-\alpha^2-\beta^2\right)^{1/2}. \quad (4)$$

The Gaussian shape of the beam is determined by the Fourier amplitudes

$$\vec{\xi}'_{\mathrm{inc}}(\alpha,\beta)=\vec{\zeta}'_{\mathrm{inc}}(\alpha,\beta)\exp[-w_0(\alpha^2+\beta^2)/4], \quad (5)$$

where the beam waist w_0 controls the lateral size of the incident beam in the focal plane.

In Eq. (3), the integration running over all possible values of α and β introduces evanescent harmonics (i.e., purely imaginary $\gamma_{(\alpha,\beta)}$) in the plane wave expansion. However, since we consider an incident beam with an oblique incidence θ leading to total reflection (Fig. 1), the radiative harmonics with a value of $\alpha<-\sqrt{\epsilon_1}\,\omega/c\cos\theta$ such that $\alpha<-\sqrt{\varepsilon_1}(\omega/c)\cos\theta$ propagate toward the negative values of z, so that they are not transmitted through the interface from the lower to the upper half space but from the upper to the lower half space. In order to keep the model within a reasonable level of complexity, we limit the integration of the 2D spectrum (3) to plane waves, for which the inequality (α^2

$+\beta^2)<\varepsilon_1(\omega^2/c^2)\cos^2\theta$ holds. With this restriction, all the harmonics in the plane wave expansion of the incident beam are radiative and travel toward the positive values of z. Note that, for our practical purpose, this approximation does not introduce any significant limitation. Indeed, assuming a beam waist as small as $w_0=\lambda$, the factor $\exp[-w_0(\alpha^2+\beta^2)/4]$ is small compared to the amplitude of the fundamental harmonic ($\alpha=\beta=0$), for any harmonic (α,β) such that $(\alpha^2+\beta^2)\geqslant\varepsilon_1(\omega^2/c^2)\cos^2\theta$, even for an angle of incidence as large as $\theta=60°$ [14]. In Eq. (3), all the plane waves are transverse; thus the component $\zeta'_{\mathrm{inc},z'}(\alpha,\beta)$ can be derived from the relation

$$\zeta'_{\mathrm{inc},z'}(\alpha,\beta)=\frac{-1}{\gamma_{(\alpha,\beta)}}[\alpha\zeta'_{\mathrm{inc},x'}(\alpha,\beta)+\beta\zeta'_{\mathrm{inc},y'}(\alpha,\beta)]. \quad (6)$$

Setting $\zeta'_{\mathrm{inc},x'}(\alpha,\beta)=1$ and $\zeta'_{\mathrm{inc},y'}(\alpha,\beta)=0$ in Eq. (3) for all possible values of α and β leads to a TM polarized beam since the electric field component $\vec{E}'_{\mathrm{inc},y'}$ perpendicular to the plane of incidence keeps a zero value at any observation point [15–17]. The TE polarization is directly obtained with $\zeta'_{\mathrm{inc},x'}(\alpha,\beta)$ and $\zeta'_{\mathrm{inc},y'}(\alpha,\beta)$ respectively fixed to 0 and 1. Note that, unlike for a single homogeneous plane wave, the electric field of a Gaussian beam is not transverse with respect to the propagation direction (the z' axis in our case), except at the focal point. As a consequence, specific effects due to this property may arise when an object is illuminated by a polarized Gaussian beam [18]. If $\mathcal{R}(\theta)$ is the usual 3×3 rotation matrix that aligns the local system of coordinates (x',y,z') with the initial reference frame (x,y,z), the expressions in the (x,y,z) system of the Fourier amplitude and the wave vector of each plane wave in the expansion (3) turn out to be

$$\begin{pmatrix}\zeta_{\mathrm{inc},x}\\ \zeta_{\mathrm{inc},y}\\ \zeta_{\mathrm{inc},z}\end{pmatrix}=\mathcal{R}(\theta)\begin{pmatrix}\zeta'_{\mathrm{inc},x'}\\ \zeta'_{\mathrm{inc},y'}\\ \zeta'_{\mathrm{inc},z'}\end{pmatrix} \quad (7)$$

and

$$\begin{pmatrix}k_x(\alpha,\beta)\\ k_y(\alpha,\beta)\\ k_z^{(1)}(\alpha,\beta)\end{pmatrix}=\mathcal{R}(\theta)\begin{pmatrix}\alpha\\ \beta\\ \gamma_{(\alpha,\beta)}\end{pmatrix}. \quad (8)$$

If δ labels the angle between the x axis of the fixed system of coordinates and the direction of $\vec{k}_{\parallel}(\alpha,\beta)=k_x(\alpha,\beta)\vec{x}+k_y(\alpha,\beta)\vec{y}$, it is a straightforward matter to show, from the boundary conditions in the plane $z=0$, that the tangential components of the transmitted Fourier amplitudes for each plane wave are obtained using

$$\begin{pmatrix}\zeta_x^{(\mathrm{T})}\\ \zeta_y^{(\mathrm{T})}\end{pmatrix}=\begin{pmatrix}(\tau_{\parallel}-\tau_{\perp})\cos^2\delta+\tau_{\perp} & (\tau_{\parallel}-\tau_{\perp})\cos\delta\sin\delta\\ (\tau_{\parallel}-\tau_{\perp})\cos\delta\sin\delta & (\tau_{\parallel}-\tau_{\perp})\sin^2\delta+\tau_{\perp}\end{pmatrix}\times\begin{pmatrix}\zeta_{\mathrm{inc},x}\\ \zeta_{\mathrm{inc},y}\end{pmatrix}. \quad (9)$$

In Eq. (9), $\tau_{\parallel}$ and $\tau_{\perp}$ are the Fresnel coefficients given by

$$\tau_{\perp}=\frac{2k_z^{(1)}(\alpha,\beta)}{k_z^{(1)}(\alpha,\beta)+k_z^{(3)}(\alpha,\beta)}, \quad (10)$$

$$\tau_{\parallel}=\frac{2\varepsilon_1 k_z^{(3)}(\alpha,\beta)}{\varepsilon_3 k_z^{(1)}(\alpha,\beta)+\varepsilon_1 k_z^{(3)}(\alpha,\beta)}. \quad (11)$$

As usual, $k_z^{(3)}$ is defined by $k_z^{(3)}(\alpha,\beta)=(\varepsilon_3\omega^2/c^2-k_x^2-k_y^2)^{1/2}$. The component $\zeta_z^{(\mathrm{T})}$ is deduced from the tangential components using the relation $\vec{\nabla}\cdot\vec{\zeta}^{(\mathrm{T})}=0$. Since all the components of $\vec{\zeta}^{(\mathrm{T})}$ are determined, the field $\vec{E}_0(x,y,z)$ is finally written as follows:

$$\vec{E}_0(x,y,z)=\int_{-\sqrt{\varepsilon_1}(\omega/c)\cos\theta}^{\sqrt{\varepsilon_1}(\omega/c)\cos\theta}d\alpha\int_{-\sqrt{\varepsilon_1(\omega^2/c^2)\cos^2\theta-\alpha^2}}^{\sqrt{\varepsilon_1(\omega^2/c^2)\cos^2\theta-\alpha^2}}d\beta\,\vec{\zeta}^{(\mathrm{T})}\times\exp[-w_0(\alpha^2+\beta^2)/4]\times\exp[i\,k_x(x-x_0)+ik_y(y-y_0)+ik_z^{(3)}(z-z_0)], \quad (12)$$

where (x_0,y_0,z_0) represents the position of the focal point in the initial, unrotated, system of coordinates (x,y,z). Let us note that the GDT requires computation of the plane wave expansion of the 3D Gaussian beam of the 0th order solution $\vec{E}_0(\vec{r})$ *only*. The direct-space discretization of the object avoids the calculation of each Fourier component of the field $\vec{E}(\vec{r})$ scattered by the SOW.

C. Illumination by a totally reflected Gaussian beam

Before discussing the optical properties of the subwavelength cross section waveguides, we first detail the illumination field that will be used to locally excite one end of a SOW. Figure 2 displays the electric intensity map computed in the (xOz) plane, using Eq. (12), for a TM polarized Gaussian beam propagating toward the negative values of x and being totally reflected on a flat glass-air interface. The electrical intensity has been normalized relative to the intensity at the focal point of the incident beam. This focal point was placed at the origin O of the fixed system of coordinates (x,y,z). An interference pattern parallel to the interface is visible in the area in which the incoming and reflected beams interact with each other. In spite of the location of the focal point at the origin of the reference frame, the incident and reflected beams are not symmetrical with respect to the $x=0$ plane. This observation is related to the Goos-Hänschen shift [19,20]. Finally, it can be seen that the incident and reflected beams appear on Fig. 2 with the same gray level intensity because the total reflection on a dielectric interface does not lead to energy losses. In the case of a metal thin film deposited on a surface, plasmon excitations may significantly reduce the intensity of the reflected beam (see Ref. [15]).

III. HOMOGENEOUS SOW'S

This section analyzes the features of the electric near-field intensity maps computed in the vicinity of homogeneous SOW's excited locally by a totally reflected Gaussian beam. These maps can be interpreted as the signal that could be

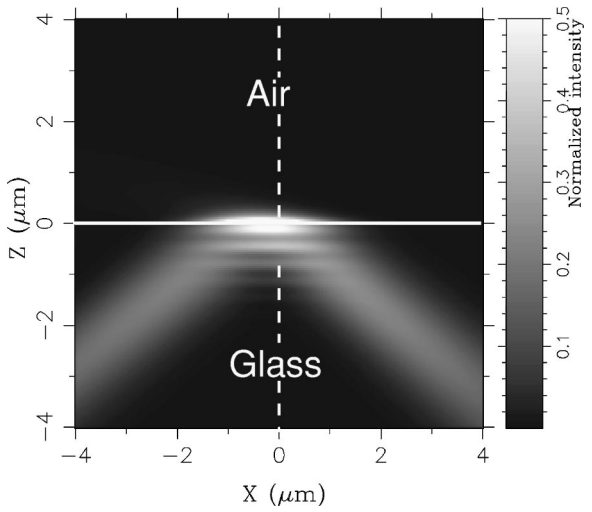

FIG. 2. Computed in the plane ($y=0$), electrical intensity of a Gaussian beam totally reflected at the interface between a glass substrate ε_1 and a less refringent outside medium ε_3 (air). The angular frequency of the incident beam defines a wavelength in vacuum $\lambda=2\pi c/\omega=633$ nm. The angle of incidence is $\theta=50°$ and the beam waist is fixed to $w_0=1.26$ μm. The intensity is normalized with respect to the intensity at the focal point ($x_0=y_0=z_0=0$)Z. The gray scale is truncated to a maximum value of 0.5 in order to visualize the interaction between the incident and reflected beams.

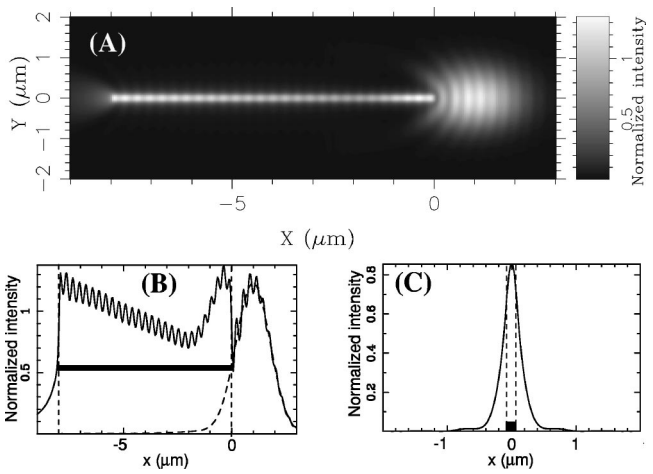

FIG. 3. (a) Top view of the electric near-field intensity computed 70 nm above a 8.0 μm long homogeneous SOW locally excited by the Gaussian beam. (b) Solid line: Crosscut of the near-field intensity map along $y=0$ μm. For reference, the dashed line shows the profile of the totally reflected beam if the SOW is absent. (c) Crosscut of the near-field intensity map along the line $x=-7$ μm. The lateral size of the device is compared to the lateral extension of the mode sustained by the SOW.

measured with a dielectric local probe of a photon scanning tunneling microscope operating in constant height mode [21]. To show the coupling of the light of the incident beam with the modes of the SOW, we consider a linear and homogeneous SOW with a length of 8 μm and a cross section of 150×150 nm^2. The SOW is supported by a transparent glass substrate with a dielectric constant $\varepsilon_1=2.25$. The dielectric constant of the SOW is fixed to a realistic value of $\varepsilon_2=4.0$ over the whole visible range. Such a value could be obtained with materials such as TiO_2 or SiN_x. The SOW is locally illuminated by a monochromatic 3D beam whose angular frequency ω defines a wavelength in vacuum $\lambda=2\pi c/\omega=633$ nm and a beam waist $w_0=2\lambda$. The three parameters, namely, the cross section, the dielectric function, and the incident angular frequency, have been chosen in such a way that the SOW could sustain a single mode if it was infinitely long and embedded in air [22]. In order to reduce the number of computational configurations to be investigated, we have restricted our analysis to a TM polarized incident beam.

Figure 3(a) presents the electric intensity map computed 70 nm above the top interface of the SOW for an incident beam propagating toward negative values of x and impinging on the substrate interface with an angle of incidence $\theta=50°$. In this example [Fig. 3(a)], the intensity is normalized with respect to the intensity existing at a point located in the observation plane just above the focal point of the beam. Revealing the excitation of a guided mode inside the SOW, an electric field intensity of the same order of magnitude as the reference intensity can be observed around the complete dielectric structure. As expected intuitively, the efficiency of this coupling is optimized when the Gaussian beam is aligned with the axis of the waveguide. We can interpret this phenomenon as a consequence of the Goos-Hänschen shift already mentioned above (Fig. 2). Actually, this lateral shift is associated with a Poynting vector of the incident beam which flows parallel to the substrate interface in the upper half medium ε_3 before coming back into medium ε_1. The SOW axis being parallel to the plane of incidence, if the right end of the SOW is placed in the area in which the Goos-Hänschen shift occurs, many Fourier components of the Poynting vector of the incident beam will be parallel to the axis of the SOW. In other words, this illumination mode achieves a kind of local source emitting light in grazing incidence. Moreover, we have observed that a good coupling efficiency is obtained when the fundamental harmonic of the beam is totally reflected. However, reducing the angle of incidence slightly below the critical angle for total reflection still allows efficient coupling provided that the beam is tightly focused. Indeed, in a tightly focused beam, the plane wave spectrum is large enough to ensure that a harmonic with a significant amplitude is totally reflected even if the angle of incidence is a few degrees below the critical angle. In the case of normal incidence, the coupling with the dielectric SOW does not occur. This normal incidence feature is quite different from what was found for metallic nanowires [4].

The crosscut plotted in Fig. 3(b) exhibits a standing wave pattern resulting from the interference of the guided mode with the light reflected back at the end of the SOW. Furthermore, in spite of the subwavelength size of the cross section of the the SOW, the mode remains well confined [see Fig. 3(c)], producing a local source of light at the left extremity of the SOW.

In order to improve the versatility needed for optical addressing, a device involving SOW components should be able to guide light not only along linear trajectories but also following bent trajectories. In today's standard optical integrated systems [23], the deflection of the propagation direction is performed with bent waveguides. However, the cur-

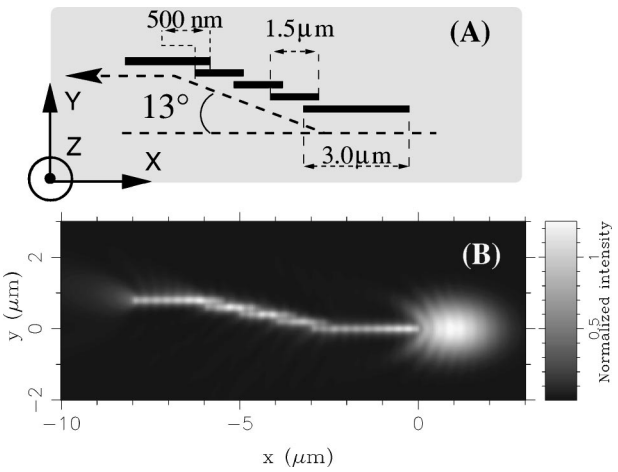

FIG. 4. (a) Arrangement of several homogeneous SOW's deposited on the surface of the substrate to guide light along a bent path. (b) Electrical near-field intensity map computed 70 nm above the system when the right-hand SOW is excited by the Gaussian beam.

vature of the bent zone must be weak in order to prevent high radiations losses. Figure 4(a) proposes an arrangement of finite-length SOW's designed to achieve an efficient deflection of light over a short transition length. This device relies on coupling the modes sustained by each single linear SOW. The lateral distance between each element has been fixed to 50 nm in order to ensure an efficient overlap of the modes of two successive elements. Figure 4(b) shows the intensity computed over the system when the incident beam illuminates the first segment only. An 800 nm lateral deflection of the light is achieved over a transition length of 3.5 μm. Relatively to standard waveguide devices, this ratio of the lateral deflection distance over the transition length appears to be rather important. Radiation losses are kept reasonably low since the intensity detected over the last segment is close to the intensity found at the end of a single linear SOW [Fig. 3(a)].

IV. HETEROGENEOUS SOW

A. Propagation along a heterogeneous SOW

The previous section considered SOW with homogeneous values of the optical index along their axis. We now examine the capability of heterogeneous SOW's to propagate a local excitation. Deposited on the same substrate as above, two homogeneous SOW's, respectively 3.0 μm and 1.5 μm long, are aligned so as to obtain a 4.5 μm gap between their closest ends (Fig. 5). A finite chain of dielectric particles is introduced in this gap. Such a chain is an elementary realization of a heterowire, which is a more general geometry defined by alternating values of the dielectric function along the longitudinal axis of the SOW. The same Gaussian beam as above excites the right end of the 3.0 μm long SOW. The light exiting at its left end then excites a heterowire. The distance between the particles is fixed at 150 nm and their dimensions along the x and z axes are, respectively, $l_x = 100$ nm and $l_z = 150$ nm. In order to study the guiding properties of the chain at the angular frequency defining $\lambda = 2\pi c/\omega = 633$ nm, we present in Fig. 6 a series of near-field intensity maps computed above the system for different

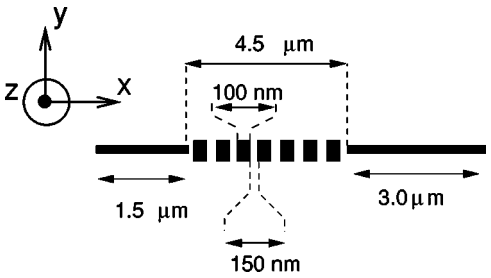

FIG. 5. Projection on the surface of the substrate of the geometry of a heterowire built as a chain of dielectric pads. The chain is placed in the gap between two homogeneous SOW's.

widths l_y of the particles. Figure 6(a) will be the reference geometry in which the gap between the two homogeneous SOW's is not padded with any particles. In spite of this gap, we observe a residual intensity over the second SOW of about 8% of the normalized intensity. This residual intensity is related to the radiative components of the field emitted by the SOW excited by the incident Gaussian beam on the right. If a chain of dielectric particles with a width of $l_y = 100$ nm [Fig. 6(b)] is inserted between the two SOW's, the intensity along the chain decays exponentially with a $1/e^2$ damping distance of about 4.0 μm. When the width l_y is scaled up to 250 nm [Fig. 6(c)], the intensity over this kind of heterowire is not damped anymore. Finally, the average intensity at the ''exit'' end of the left SOW is found to be

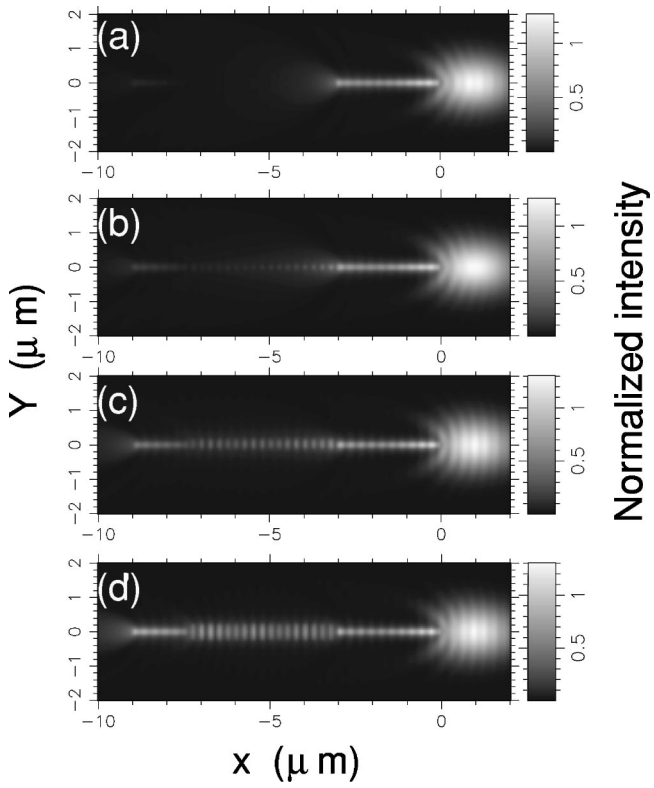

FIG. 6. Sequence of near-field electrical intensity maps computed over the system described in Fig. 5 for increasing values of the lateral sizes l_y of the particles. For reference, in (a), the gap between the two homogeneous SOW's is devoid of particles. Dielectric particles of increasing size (l_y along the y axis) are padding the gap in (b) ($l_y = 100$ nm), (c) ($l_y = 250$ nm), and (d) ($l_y = 450$ nm).

equal to the average intensity computed over the ''entrance'' end of the SOW when the width l_y reaches about 450 nm [Fig. 6(d)]. We conclude that mesoscopic dielectric particles, aligned in coplanar geometry, can propagate a local excitation over distances of several micrometers with a reasonably low damping.

Of course, it is clear that the region located between the two homogeneous SOW's is not a true optical gap because, as shown in Fig. 6(a), some residual radiative components are emitted at the end of the right SOW. However, as in the case of incomplete optical gaps [7,8], the introduction of heterowires between the two homogeneous SOW's introduces additional electromagnetic states which are available to improve the amount of transferred energy. These electromagnetic states are localized around each individual particle. By overlapping each other, they can propagate a local excitation along the chain. Figure 6 demonstrates that increasing the lateral sizes of the particles improves the propagation along the chain, thereby increasing the output intensity at the ''exit'' end of the left SOW. This is due not only to the overlap of the localized states but also to the more efficient forward scattering of the radiative components, which is expected when the volume of a scatterer grows [24].

B. Spectroscopic properties of periodic heterowires

The above results show that an appropriate choice of the size of the small dielectric particles may define a heterowire guiding visible light over several micrometers. As introduced in Ref. [7] and as will be detailed in the next section, such an effect is obtained by increasing, in a desired range of incident angular frequencies, the density of states of a poorly transmitting structure chosen as reference. Recent works about photonic band gap materials [25] follow another route: fine tuning of the periodic modulation of the dielectric function is exploited to decrease the density of electromagnetic states of a transparent reference system in a desired range of incident angular frequencies. Both approaches are, of course, equivalent since they both aim at tailoring the transmission spectrum.

In order to get more insight into spectroscopic properties, Fig. 7 considers 11 identical particles aligned to set a 5 μm long chain. A spacing of 150 nm separates the 150 nm high particles whose projections on the surface of the substrate define 350×350 nm^2 squares. The index of refraction of these pad-shaped particles is equal to 2. Keeping the same normalization procedure as above, Fig. 7 displays the electric intensity computed at an observation point located at the ''exit'' left end of the chain when the incident angular frequency defines $\lambda=2\pi c/\omega$ varying between 450 nm and 800 nm. The spectrum of Fig. 7 exhibits a narrow gap centered around 550 nm that corresponds to the low-transmission regime. Such a spectral signature is similar to the effect required when introducing a periodic structure in order to tailor photonic band gaps in the transmission spectrum of semiconductor waveguides [26,27]. The observed gap is related to a kind of destructive interference pattern between the fields scattered back and forth by each particle.

Figure 8 displays two near-field electric intensity maps computed close above the chain for two incident angular frequencies defining $\lambda=2\pi c/\omega=543$ nm and 633 nm corresponding, respectively, to a minimum and a maximum in the transmission spectrum. For $\lambda=543$ nm, the intensity decays strongly before reaching the ''exit'' end of the heterowire while, for $\lambda=633$ nm, an important intensity is spread over the whole chain. For $\lambda=633$ nm, the intensity over the particles is enhanced right over their edges, which are perpendicular to the longitudinal axis of the chain. This pattern features the mode sustained by each particle. Considering now the response of the entire chain, we observe that the individual response of the particles is modulated by an enve-

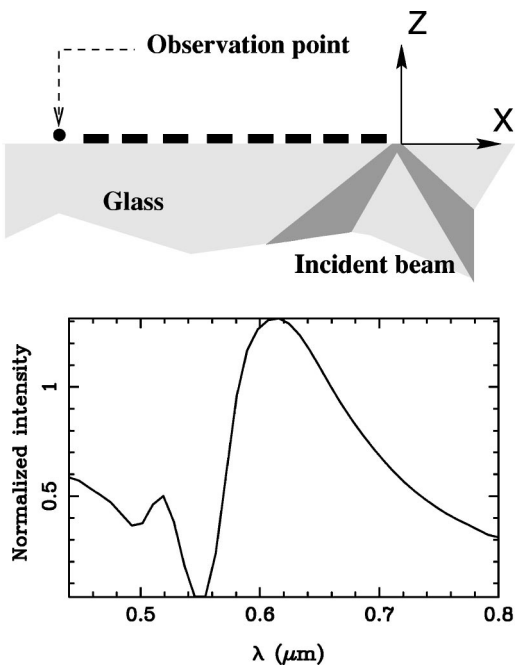

FIG. 7. Near-field transmission spectrum of a chain of mesoscopic particles (parameters described in the text). The normalized intensity corresponds to the electric intensity at the observation point at the left ''exit'' end of the chain.

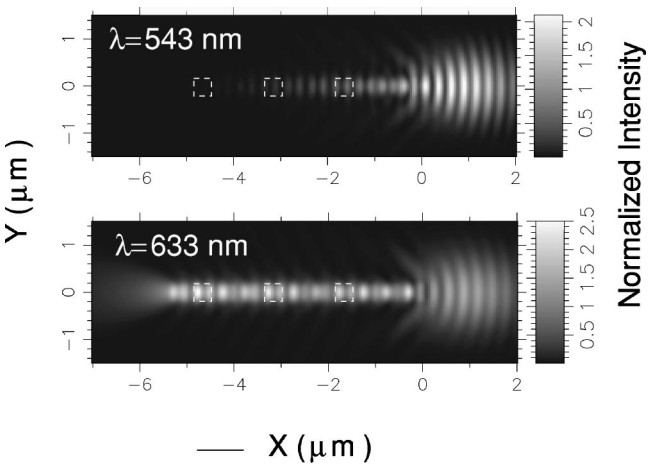

FIG. 8. Near-field electrical intensity map computed over the chain whose near-field transmission spectrum appears in Fig. 7. The angular frequencies defining the wavelengths in vacuum $\lambda=2\pi c/\omega=543$ nm and 633 nm correspond, respectively, to a minimum and a maximum of the transmission spectrum of Fig. 7. In order to avoid overloading the figure, the projections of only three particles in the chain are shown on both maps.

lope function with a periodicity of about 1.5 μm. This modulation is obviously related to the back reflection at the end of the finite-length chain. Both the size of the individual particles and the length of the entire chain determine the spatial distribution of the electric field and consequently the spectroscopic properties of the device. A previous study [7] found that the position and width of the gap in the transmission spectrum of a heterowire integrated in coplanar geometry are sensitive to the geometrical parameters, the refractive index, and the number of particles in the chain. The filtering of a given angular frequency is thus possible by adjusting these parameters.

V. ELECTROMAGNETIC LOCAL DENSITY OF STATES

The electromagnetic local density of states is the basic underlying concept that describes the intrinsic optical properties of heterowires, without any additional features due to any specific illumination. The Green function approach to scattering theory, adopted in this paper, implicitly relies on the LDOS $\eta(\vec{r},\omega)$, which reads [28]

$$\eta(\vec{r},\omega) = -\frac{1}{\pi}\mathrm{Tr}\,\mathrm{Im}\;\overleftrightarrow{G}(\vec{r},\vec{r},\omega) \tag{13}$$

where the tensor $\overleftrightarrow{G}(\vec{r},\vec{r}',\omega)$ is the Green dyadic of the whole system defined as any structure deposited on the surface of the substrate. When dealing with complex optical systems such as those considered here, the precise computation of the electromagnetic dyadic $\overleftrightarrow{G}(\vec{r},\vec{r}',\omega)$ is obtained by solving the Dyson equation that relates $\overleftrightarrow{G}(\vec{r},\vec{r}',\omega)$ to the Green dyadic $\overleftrightarrow{G}_{\mathrm{ref}}(\vec{r},\vec{r}',\omega)$ of the reference system [7]. Defined as in Eq. (13), the LDOS computed in this paper represents the spatial distribution of the electric intensity associated with the eigenstates, of angular frequency ω, sustained by a structure deposited on the surface of the substrate.

In order to illustrate the information contained in LDOS maps, let us consider two homogeneous SOW's with similar parameters (length 5 μm, width 150 nm) except for the height, which is fixed to $h=100$ nm for the first one and to $h=150$ nm for the second one. Figures 9 and 10 display simultaneously the spatial distribution of electric field intensity and the LDOS maps, both computed in an observation plane located 70 nm over the top of each SOW. The electrical intensity maps are computed for a local illumination produced by a totally reflected Gaussian beam with an incident angular frequency defining $\lambda = 2\pi c/\omega = 633$ nm. The 100 nm high SOW does not sustain a guided mode at this specific frequency, since only a very weak intensity is found at the exit end of the SOW [Fig. 9(a)]. On the contrary, the near-field intensity map computed above the 150 nm high waveguide shows that the higher SOW propagates a local excitation [Fig. 10(a)]. Looking now to the corresponding LDOS maps above each SOW, a rather flat response is spread along the axis of the smaller SOW [Fig. 9(b)] while a pronounced standing wave shows up along the axis of the higher one [Fig. 10(b)]. As in the case of the field intensity map presented in Fig. 3, the standing wave pattern in the LDOS is caused by the finite length of the structure which allows resonant multiple reflections at both ends of the SOW. Such

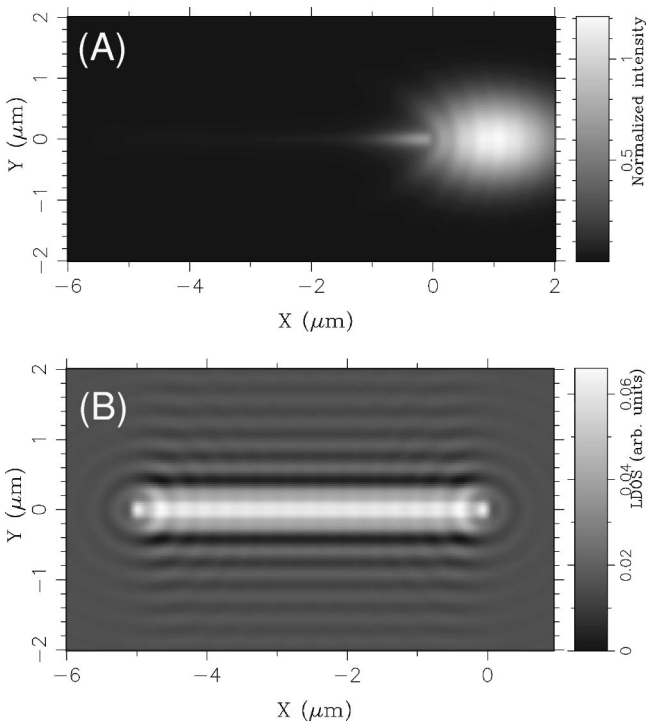

FIG. 9. Comparison of the near-field intensity ($|\vec{E}|^2$) maps (a) and LDOS maps (b) computed in the same plane of observation above a 100 nm high homogeneous SOW.

a resonant phenomenon is, of course, identified with a mode with a larger lifetime at this specific angular frequency. We thus conclude that a significantly pronounced standing wave pattern showing up in the LDOS map determines a kind of

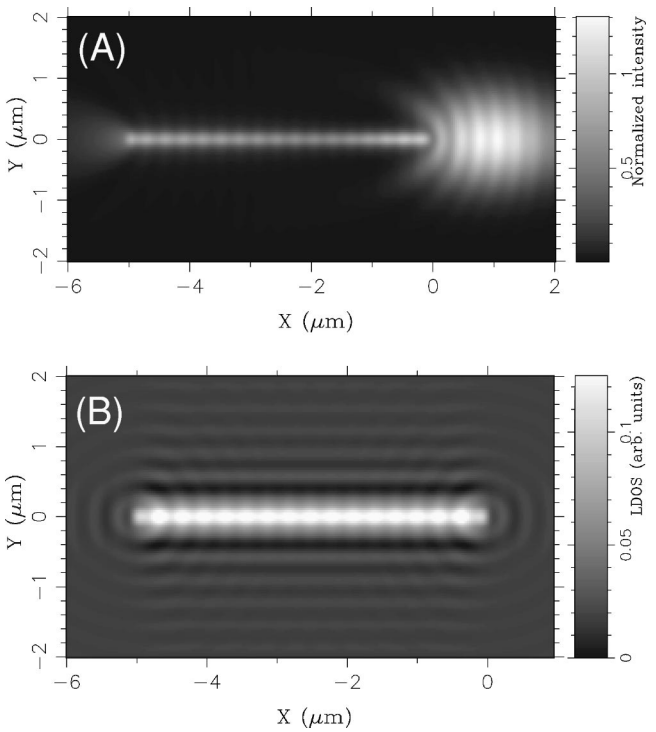

FIG. 10. Comparison of the near-field intensity ($|\vec{E}|^2$) maps (a) and LDOS maps (b) computed in the same plane of observation above a 150 nm high homogeneous SOW.

eigenmode of the system. This reasoning can also be applied to studying the spectral properties of heterowires. Note that the simple criterion discussed here is somewhat arbitrary since it depends on the observation plane (70 nm above the top of each SOW in our examples). A more thorough criterion, taking into account the LDOS values *inside* the SOW, should indeed be elaborated to analyze the optical eigenmodes of any SOW device. Nevertheless, having in mind to check the optical properties of a SOW by near-field optical measurements justifies the choice of the criterion retained here.

VI. CONCLUSION

Numerical simulations based on the Green dyadic method show that the excitation of SOW's made of dielectric structures integrated in coplanar geometry is conceivable using a 3D Gaussian beam totally reflected at the interface of the substrate. For visible frequencies, the guiding process is expected to be efficient over distances of several micrometers.

Computations of near-field electrical intensity maps suggest that a homogeneous SOW, locally excited at one of its ends by a 3D Gaussian beam totally reflected at the interface of the substrate, provides a source of light confined within a subwavelength lateral size at its other end. Such a local source could be used to address optically single nano-objects (fluorescing molecules, quantum dots, etc.). In addition, relevant guiding processes along curved paths with small radii of curvature have been identified.

The structure of the the dielectric function profile of the SOW along its linear axis allows one to tailor the frequency ranges where the propagation occurs. In such heterowires, the propagation relies on overlapping of the localized states sustained by each particle inside the heterowire. For sufficiently large particles, a phenomenon akin to a photonic band gap effect can be found in the near-field transmission spectrum of a heterowire deposited on a substrate. Finally, the electromagnetic local density of states may provide relevant insight into the optical properties of SOW devices with no need to resort to any local illumination model.

ACKNOWLEDGMENTS

The CEMES is CNRS UPR No. 8011. The LPUB is CNRS UMR No. 5027. This work benefited from the financial support of the Region of Burgundy and of the French Ministère de l'Education Nationale, de la Recherche et de la Technologie.

[1] A. Dereux, C. Girard, and J.C. Weeber, J. Chem. Phys. **112**, 7775 (2000).
[2] J. Takahara, S. Yamagishi, H. Taki, A. Morimoto, and T. Kobayashi, Opt. Lett. **22**, 475 (1997).
[3] M. Quinten, A. Leitner, J.R. Krenn, and F.R. Aussenegg, Opt. Lett. **23**, 1331 (1998).
[4] J.C. Weeber, A. Dereux, C. Girard, J.R. Krenn, and J.P. Goudonnet, Phys. Rev. B **60**, 9061 (1999).
[5] D. Courjon, C. Bainier, Ch. Girard, and J.M. Vigoureux, Ann. Phys. (Paris) **2**, 149 (1993).
[6] C. Girard, A. Dereux, and C. Joachim, Europhys. Lett. **44**, 686 (1998).
[7] C. Girard, A. Dereux, and C. Joachim, Phys. Rev. E **59**, 6097 (1999).
[8] D. Mulin, M. Spajer, D. Courjon, F. Carcenac, and Y. Chen, J. Appl. Phys. **87**, 534 (2000).
[9] C. Girard and A. Dereux, Rep. Prog. Phys. **59**, 657 (1996).
[10] R. Carminati and J.J. Greffet, Phys. Rev. Lett. **82**, 1660 (1999).
[11] C. Girard and X. Bouju, J. Opt. Soc. Am. B **9**, 298 (1992).
[12] A.A. Maradudin and D.L. Mills, Phys. Rev. B **11**, 1392 (1975).
[13] A.D. Yaghjian, Proc. IEEE **68**, 248 (1980).
[14] E.M. Khaled, C.H. Hill, and P.W. Barber, IEEE Trans. Antennas Propag. **41**, 526 (1995).
[15] D. Van Labeke, F. Baida, and J.M. Vigoureux, Ultramicroscopy **71**, 351 (1998).
[16] F. Baida and D. Van Labeke, Phys. Rev. B **60**, 7812 (1999).
[17] F. Baida, D. Van Labeke, and J.M. Vigoureux, Opt. Commun. **171**, 317 (1999).
[18] F. Baida, D. Barchiesi, and D. Van Labeke, Opt. Lett. **24**, 1587 (1999).
[19] S. Kosaki and H. Sakurai, J. Opt. Soc. Am. **68**, 508 (1978).
[20] A. Madrazo and M. Nieto-Vesperinas, Opt. Lett. **20**, 2445 (1995).
[21] R.C. Reddick, R.J. Warmack, and T.L. Ferrel, Phys. Rev. B **39**, 767 (1989).
[22] J.E. Goell, Bell Syst. Tech. J. **48**, 2133 (1969).
[23] W.K. Burns and A.F. Milton, in *Guided-Wave Optoelectronics*, edited by T. Tamir (Springer, Berlin, 1988), pp. 89–144.
[24] C.G. Bohren and D.R. Huffman, in *Absorption and Scattering of Light by Small Particles*, edited by A.D. Boardman (Wiley, New York, 1983).
[25] E. Yablonovitch, Phys. Rev. Lett. **58**, 2059 (1987).
[26] P.R. Villeneuve, S. Fan, J.D. Joannopoulos, K. Lim, J.C. Chen, G.S. Petrich, L.A. Kolodziejski, and R. Reif in *Photonic Band Gap Materials*, edited by C. M. Soukoulis (Kluwer, Dordrecht, 1996), pp. 416–421.
[27] J.S. Foersi, P.R. Villeneuve, J. Ferrera, E.R. Thoen, G. Steinmeyer, S. Fan, J.D. Joannopoulos, L.C. Kimerling, H.I. Smith, and E.P. Ippen, Nature (London) **390**, 143 (1997).
[28] E.N. Economou, *Green's Function in Quantum Physics* (Springer, Berlin, 1983).